We are IntechOpen, the world's leading publisher of Open Access books Built by scientists, for scientists

6,900
Open access books available

185,000
International authors and editors

200M
Downloads

Our authors are among the

154
Countries delivered to

TOP 1%
most cited scientists

12.2%
Contributors from top 500 universities



WEB OF SCIENCE™

Selection of our books indexed in the Book Citation Index in Web of Science™ Core Collection (BKCI)

Interested in publishing with us?
Contact book.department@intechopen.com

Numbers displayed above are based on latest data collected.
For more information visit www.intechopen.com



7

Quantum-Chemical Design of Molecular Quantum-Dot Cellular Automata (QCA): A New Approach from Frontier Molecular Orbitals

Ken Tokunaga
General Education Department, Faculty of Engineering, Kogakuin University
Japan

1. Introduction

Recently, research and development of next-generation devices have been very active (1). Quantum-dot cellular automata (QCA) (2) which is constructed from many quantum dot cells (QDC, Fig. 1) is one of such new-generation devices. The QCA devices such as a majority logic gate and a signal transmission wire (Fig. 2) are expected to achieve a dramatic saving of energy and an increase in processing speed of computing since these devices are free from a current flow. Successful operations of several QCA devices have been already demonstrated (3; 4). However, for improvement in operation temperature and size of the QCA devices, the idea of molecular quantum-dot cellular automata (molecular QCA) devices (5), in which a QDC constructed from small metallic dots is replaced by a single molecule, was proposed. Toward the experimental operation of molecular QCA devices, syntheses of tetranuclear complexes (6–10) and simplified dinuclear complexes (11; 12), and single-molecule observation of the dinuclear complexes (13–16) have been paid attention. However, the capacity of molecular QCA devices for molecular computing is still not clear.

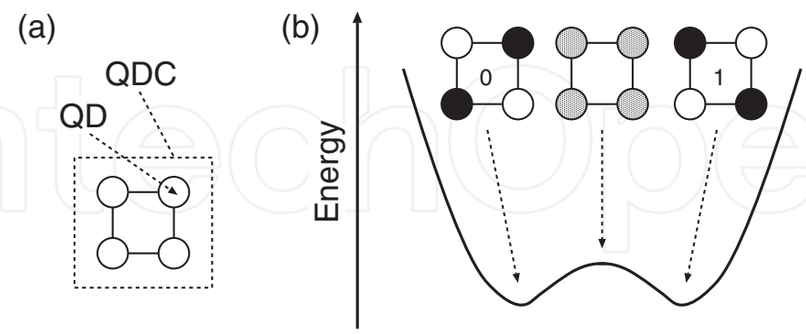


Fig. 1. (a) Quantum dot (QD) and quantum-dot cell (QDC) constructed from four QDs. (b) Schematic energy curve of two localized degenerate states, "0" and "1", and one delocalized transition state of QDC after injection of two electrons into QDC. Charge of open circles is positive relative to that of filled circles. In the transition state, charges of four dots are all equivalent.

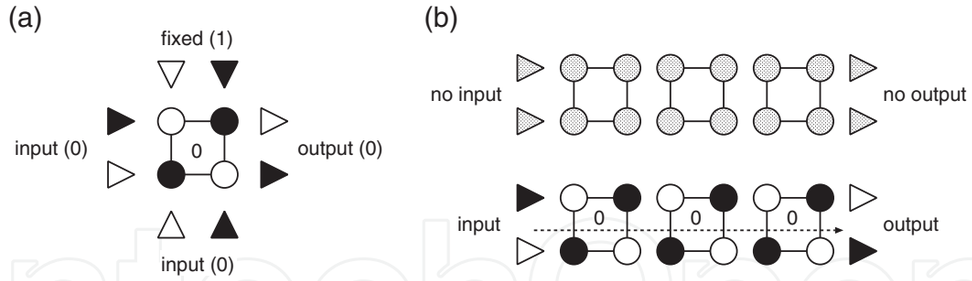


Fig. 2. Examples of QCA devices constructed from many QDCs: (a) QCA logic gate (OR gate) and (b) QCA signal transmission wire.

Braun-Sand and Wiest (17; 18) have reported theoretical studies on the electronic response of Ru dinuclear complexes to Li^+ in order to propose molecular QCA candidates. Lent *et al.* took up hydrocarbons with allyl end-groups (19; 20) and tetranuclear complex (21). In these studies, however, only the static response of molecular QCA to the switch of input was focused, and dynamic properties such as signal transmission time after the switch had not been discussed. About this point, Timler and Lent (22), and Lu and Lent (23) have reported the dynamic behavior of multi-cellular systems using model Hamiltonian. However, the detailed discussion about a relation between the electronic structure and dynamic properties had not been made in their studies. For understanding the behavior and performance of molecular QCA devices and development of high-efficient devices, it is necessary to clear the relation.

Very recently, I have proposed the simple method for an analysis of dynamic behavior of QCA devices, taking Creutz-Taube complexes $[L_5M\text{-}BL\text{-}ML_5]^{n+}$ (M=Ru, BL=pyrazine(**py**) and 4,4′-bipyridine(**bpy**), L=NH_3, n=5) as examples (24), based on the methods proposed by Remacle and Levine (25; 26). These analyses are all based on the simple one electron theories, density functional theory (DFT) and Hartree-Fock theory (HF). Time evolution of the wave function is expressed by the *initial* and *final* stationary states. *Initial* wave function is expanded by *final* wave function. Using this method, main properties concerning the signal transmission such as the signal period T, the signal amplitude A, and the signal transmission time t_{st} (see Fig. 3) can be interpreted as follows (24):

- Signal period (T) is inverse proportional to an orbital energy gap, $\Delta\varepsilon_{HL}$, between HOMO (the highest occupied molecular orbital, H) and LUMO (the lowest unoccupied molecular orbital, L) of the *final* stationary state.
- Signal amplitude (A) is proportional to an overlap integral, $d_{LH'}$, between HOMO of the *initial* stationary state (H') and LUMO of the *final* stationary state (L).
- Signal transmission time (t_{st}) is determined depending on the balance of A and T.

This method has advantage that signal transmission behavior can be analyzed from the viewpoint of one electron properties, which are shapes of molecular orbitals (MOs) and MO energies. Thus, the proposed method is suitable for simple design of high-performance molecular QCA. Additionally, in my next paper (27), metal-dependence of dynamic behavior of signal transmission through metal complexes $[L_5M\text{-}BL\text{-}ML_5]^{n+}$ (M=Fe, Ru, and Os, BL=**py** and **bpy**, L=NH_3, n=5), was discussed.
In this Chapter, I review my approaches (24; 27) for the theoretical study on the two-site molecular QCA (Fig. 3) . Additionally, I discuss the influence of complex charge n on the signal transmission through molecular QCA. The reason why mixed-valence complexes are

suitable for molecular QCA is shown from the calculation of complexes with charge n=4, 5, and 6. Summarizing these results, I propose a new and simple approach for designing high-performance molecular QCA.

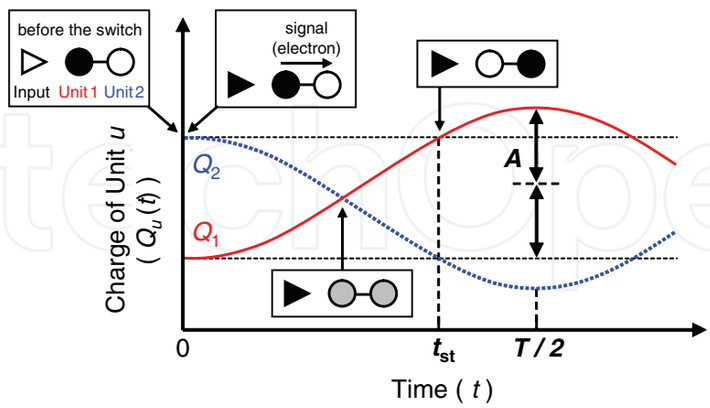


Fig. 3. Simplified two-site QCA and schematic picture of signal transmission between two units after the switch of input. A, T, and t_{st} are the signal amplitude, the signal period, and the signal transmission time, respectively.

This Chapter is organized as follows. In section 2, model, theory, and computational method of dynamic simulations are presented. A detailed explanation about the time evolution of the Mulliken charge (28) is also given. Calculated results of geometric parameters and molecular orbitals of selected complexes are shown in section 3. In section 4, the dynamic responses of molecular QCA cell upon the switch are calculated by the DFT and HF methods. In subsection 4.1, the relation between "input position" and signal transmission behavior is discussed. Detailed procedure of analysis from MOs are explained in this subsection. Relation between "switch power" and signal transmission behavior is shown in subsection 4.2. "Complex charge" also have great influence on the signal transmission (subsection 4.3). Lastly in subsection 4.4, the influence of "metal kind" on the signal transmission is discussed. In all subsections of section 4, factors which determine the dynamic properties of molecular QCA cell are discussed from the viewpoint of MOs and orbital energies. Finally, this Chapter is summarized in section 5.

2. Model, theory, and computation

2.1 Model

Schematic picture of signal transmission behavior is shown in Fig. 3. Before the switch (input charge is positive), unit 1 (U1) and unit 2 (U2) have negative and positive charges, respectively. U1 is constructed from one M atom near to the input plus five NH_3 ligands, and U2 is constructed from one M atom far from the input plus five NH_3 ligands (see Fig. (4). The moment of the switch of input corresponds to t=0. After the switch of the input charge from q^i to q^f, as time flows after the switch, $Q_2(t)$ decreases and $Q_1(t)$ increases, namely, signal (electron) is transmitted from U1 to U2 by the Coulombic repulsion. Via transition state, signal transmission is completed when Q_1 becomes almost same to $Q_2(t=0)$, and Q_2 becomes almost same to $Q_1(t=0)$. This time is called the signal transmission time (t_{st}). After the signal transmission, periodic behavior is repeated with a period of T and an amplitude of A.

Like the previous work by Braun-Sand and Wiest (18), dinuclear metal complexes shown in Fig. 4 are used to understand the essence of signal transmission through the molecular QCA cell. Bridging ligand (BL) of the complexes is pyrazine (**py**) or 4,4′-bipyridine (**bpy**), and ligand is NH_3. Total charge of the whole molecule is $n+$, excluding the input charge. Metal atoms (M) are selected as Fe, Ru, and Os and charges ($n+$) of the complexes are 4+, 5+, and 6+. These complexes are well-known to have mixed-valence electronic state when $n = 5$, and such complexes are called Creutz-Taube complexes (29; 30). Point charge q placed parallel to M-N_{BL} axis at a distance of r_{q-M} = 5, 10, and 15 Å from the M atom is used as an input to the complexes. For the discussion of switch power, three kinds of switch patterns, (q^i, q^f) = (+0.1, -0.1), (+0.3, -0.3), (+0.5, -0.5) (in e unit), are selected.

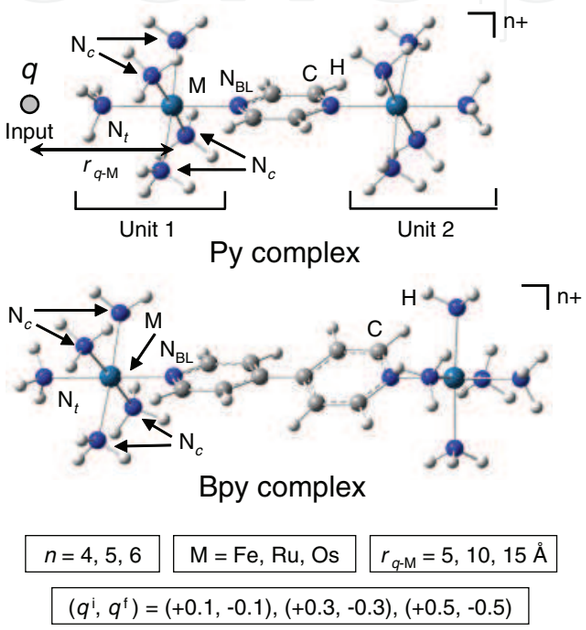


Fig. 4. Input and structures of **py** and **bpy** complexes.

2.2 Theory

Dynamic calculation for the simulation of signal transmission is all based on one-electron theories. A method of time evolution is similar to that of Remacle and Levine (24–27). All procedures shown below are repeated for both α and β MOs.

In *initial* stationary state before the switch, the following one-electron equation

$$h^{\mathrm{i}}|\psi_n^{\mathrm{i}}\rangle = \varepsilon_n^{\mathrm{i}}|\psi_n^{\mathrm{i}}\rangle \tag{1}$$

is satisfied, where h^{i}, $|\psi_n^{\mathrm{i}}\rangle$, and $\varepsilon_n^{\mathrm{i}}$ denote one-electron Hamiltonian, nth MO, and nth orbital energy when q=q^{i}, respectively. Similarly, in *final* stationary state after the switch, the following equation

$$h^{\mathrm{f}}|\psi_n^{\mathrm{f}}\rangle = \varepsilon_n^{\mathrm{f}}|\psi_n^{\mathrm{f}}\rangle \tag{2}$$

is satisfied, where h^{f}, $|\psi_n^{\mathrm{f}}\rangle$, and $\varepsilon_n^{\mathrm{f}}$ denote one-electron Hamiltonian, nth MO, and nth orbital energy when q=q^{f}, respectively. At the moment ($t = 0$) of switch of input (q=$q^{\mathrm{i}} \rightarrow q$=$q^{\mathrm{f}}$),

one-electron Hamiltonian h suddenly changes from h^{i} to $h^{\mathrm{f}}(0)$ (31) but MOs are remaining $|\psi_n^{\mathrm{i}}\rangle$, so that time evolution of nth MO $|\psi_n(t)\rangle$ is represented by the following time-dependent Schrödinger equation (in atomic unit)

$$i\frac{\partial|\psi_n(t)\rangle}{\partial t} = h^{\mathrm{f}}(t)|\psi_n(t)\rangle, \tag{3}$$

where $|\psi_n(0)\rangle$ corresponds to $|\psi_n^{\mathrm{i}}\rangle$. Neglecting the time dependence of $h^{\mathrm{f}}(t)$ (assumed to be equal to h^{f} of Equation 2) and expanding $|\psi_n(t)\rangle$ in a complete set of the *final* stationary states $|\psi_j^{\mathrm{f}}\rangle$ of Equation 2, $|\psi_n(t)\rangle$ is written as

$$|\psi_n(t)\rangle = e^{-ih^{\mathrm{f}}t}|\psi_n(0)\rangle = \sum_j^{\mathrm{all}} e^{-ih^{\mathrm{f}}t}|\psi_j^{\mathrm{f}}\rangle\langle\psi_j^{\mathrm{f}}|\psi_n(0)\rangle = \sum_j^{\mathrm{all}}|\psi_j^{\mathrm{f}}\rangle e^{-i\varepsilon_j^{\mathrm{f}}t}d_{jn}, \tag{4}$$

where $d_{jn} = \langle\psi_j^{\mathrm{f}}|\psi_n(0)\rangle = \langle\psi_j^{\mathrm{f}}|\psi_n^{\mathrm{i}}\rangle$ is the overlap integral between MOs and j runs over all MOs when $q = q^{\mathrm{f}}$. This approximation gives not only a drastic reduction of computational time but also a simple picture of signal transmission based on MOs. Then, an inner product of $|\psi_n(t)\rangle$ is

$$\langle\psi_n(t)|\psi_n(t)\rangle = \sum_{j,j'}^{\mathrm{all}} d_{jn}d_{j'n}e^{i\Delta\varepsilon_{jj'}t}\langle\psi_j^{\mathrm{f}}|\psi_{j'}^{\mathrm{f}}\rangle = 1, \tag{5}$$

where $\Delta\varepsilon_{jj'} = \varepsilon_j^{\mathrm{f}} - \varepsilon_{j'}^{\mathrm{f}}$. In actual calculation, $|\psi_j\rangle$ and $|\psi_{j'}\rangle$ are expressed by localized gaussian functions $|\phi\rangle$ and molecular coefficients c as

$$|\psi_j\rangle = \sum_\mu^{\mathrm{all}} c_{j\mu}|\phi_\mu\rangle, \tag{6}$$

$$|\psi_{j'}\rangle = \sum_\nu^{\mathrm{all}} c_{j'\nu}|\phi_\nu\rangle, \tag{7}$$

where μ and ν run over all basis functions. Total number of electrons N is defined as

$$N = \sum_n^{\mathrm{occ.}}\langle\psi_n(t)|\psi_n(t)\rangle. \tag{8}$$

Substituting Equations 5 and 7 into Equation 8, N can be explicitly rewritten like the form of Mulliken population as (32; 33)

$$\begin{aligned} N &= \sum_{\mu,\nu}^{\mathrm{all}}\left[\sum_n^{\mathrm{occ.}}\sum_{j,j'}^{\mathrm{all}} d_{jn}d_{j'n}\cdot c_{j\mu}c_{j'\nu}\cdot\cos(\Delta\varepsilon_{jj'}t)\right]\langle\phi_\mu|\phi_\nu\rangle \\ &= \sum_{\mu,\nu}^{\mathrm{all}} P_{\nu\mu}S_{\mu\nu} = \sum_\nu^{\mathrm{all}}(\mathbf{PS})_{\nu\nu}, \end{aligned} \tag{9}$$

where $\mathbf{S}$ is an overlap matrix of $S_{\mu\nu}(=\langle\phi_\mu|\phi_\nu\rangle)$, and $\mathbf{P}$ is a population matrix of $P_{\nu\mu}$:

$$P_{\nu\mu} = \sum_n^{\mathrm{occ.}}\sum_{j,j'}^{\mathrm{all}} d_{jn}d_{j'n}\cdot c_{j\mu}c_{j'\nu}\cdot\cos(\Delta\varepsilon_{jj'}t). \tag{10}$$

Then, the time-dependent Mulliken charge of unit u is defined as

$$Q_u(t) = \sum_{a \in u}^{\text{Atom}} \left\{ Z_a - \sum_{\nu \in a}^{\text{Basis}} (\mathbf{PS})_{\nu\nu} \right\}, \tag{11}$$

where Z_a is a nuclear charge of an atom a. The value in the braces of Equation 11 corresponds to the Mulliken charge of a.

2.3 Computation

All dynamic calculations were performed by the restricted DFT method for 4+ and 6+ complexes, and unrestricted DFT method for 5+ complexes, using B3LYP functional. It is well-known that DFT method generally over-estimate the electron delocalization (35), so that the HF method which generally under-estimate the electron delocalization was also checked. However, detailed results of HF method are not shown in this chapter (see my previous paper, ref. 24). Conventional basis set was used for H, C, and N atoms (6-31G(d) for C and N atoms, and 6-31G for H atoms). All-electron 3-21G basis set was used for Fe and Ru atoms, and LANL2DZ basis set and LANL2 pseudo potential were used for Ru and Os atoms. It was confirmed about Ru complexes that there is only a small difference between the results obtained by 3-21G and LANL2DZ basis sets. Therefore, the comparison between Fe (3-21G), Ru (3-21G), and Os (LANL2DZ) complexes will be valid. All results of Ru complexes shown in this chapter are those obtained by 3-21 basis set for Ru atom.
Gaussian 03 program package (34) was used for geometrical optimizations and self-consistent field electronic calculations. Fortran 77 program for the time evolution of the Mulliken charge and its analysis was coded by myself.

3. Structures

3.1 Geometries

Geometrical optimizations were performed for only 5+ complexes. The schematic structures of **py** and **bpy** complexes with are shown in Fig. 4. N_{BL}, N_c, and N_t represent N atoms of M-BL, *cis*-M-NH_3, and *trans*-M-NH_3 bonds, respectively. Geometrical optimizations of **py** and **bpy** complexes have already been studied by other research groups, imposing or without imposing symmetry (35–39). In this chapter, all possible symmetries (including C_1 point group) were checked in the search of the stable structures, and it was confirmed that the most stable structures have no vibrational modes with imaginary frequencies.
Table 1 shows a summary of the computed geometries of this work. For **py** complex, imposing C_{2h}, C_{2v}, C_2, C_s, and C_i symmetries, the most stable symmetries were obtained as C_{2h} symmetry (^2B_g state) for Ru complex and C_2 symmetry (^2B state) for Fe and Os complexes. Some calculations starting from C_1 symmetry also converged into these symmetries, so that stable structures of **py** complex were concluded to be symmetric. Energy differences between the most stable structures in each symmetry are very small that the symmetry of the stable structure will strongly depend on a selection of calculation method and basis set. Two M atoms of the complex are equivalent so that **py** complexes are regarded as Class III of Robin-Day's classification (40). The results of this work about Ru complexes are very similar to the results obtained by Braun-Sand and Wiest (17), but Ru-N_{BL} bond lengths are estimated a little longer due to the polarization basis function of N atoms. Compared with X-ray crystal structure (42; 43), computed bond lengths, especially Ru-N_{BL} bond length, are over-estimated

by about 0.2 Å. This is because that inter-molecular interactions are neglected in calculations of this article.

	py			**bpy**		
Metal	Fe	Ru	Os	Fe	Ru	Os
Symmetry	C_2	C_{2h}	C_2	C_2	C_2	C_2
Electronic State	^2B	^2B_g	^2B	^2B	^2B	^2B
M-N_{BL}	1.939	2.206	2.099	1.927	2.169	2.115
M-N_c	2.028	2.210	2.197	2.026	2.205	2.192
M-N_t	2.075	2.191	2.211	2.071	2.208	2.214
dihedral angle	-	-	-	15.1	28.3	23.0

Table 1. Summary of symmetries, irreducible representations of electronic state, and computed M-N bond lengths (Å) of **py** and **bpy** complexes with charge $n = 5$. M-N_c bond length is averaged over all M-N_c bonds.

For **bpy** complex, the most stable symmetries finally converged to C_2 symmetry (^2B state). Another structure starting from C_1 symmetry also converged into this structure, so that C_2 symmetry was concluded to be the most stable structure. Computed bond lengths of Ru complexes in Table 1 is similar to the results obtained by Braun-Sand and Wiest (17). The dihedral angles between two C_5N rings are 15.1°, 28.3°, and 23.0° for Fe, Ru, and Os complexes, respectively. These calculation predicts **bpy** complex to be classified into Class III. Contrast to above results by DFT method, HF method gives C_1 symmetry as stable structure of **bpy** complexes (not shown in the text)(24). HF calculation predicts large difference between two M-N_{BL} bond lengths. This result is consistent with the fact that Ru-**bpy** complex is thought to belong to Class II due to the experimental result of near-IR spectrum (41). These calculated results are not surprising because HF method tends to give more localized electronic structures than DFT method.
In my previous paper (24), **bpy** complexes were classified into Class III and Class II by DFT and HF methods, respectively. And it was found that signal transmission does not take place in Class II complex by HF method. Therefore, I focused only on the Class III result by DFT method in order to analysis signal transmission behavior and expand knowledge about molecular design of QCA even though the classification of **bpy** complex into Class III is contradict to the experimental observation.

3.2 Frontier molecular orbitals

Frontier molecular orbitals of Ru complexes (BL = **py** and **bpy**, $n = 5$) are shown in Fig. 5. Be careful that no input charge is put at the side of complex in this figure. Other orbitals do not contribute to the signal transmission so that are not shown here. For **py** complexes, 112α and 113α orbitals are linear combinations of $4d_{x^2-y^2}$ orbitals of Ru atoms. 112β and 113β orbitals are constructed from $4d_{yz}$ orbitals of Ru atoms and π^* orbital of BL. In 112β orbitals, $4d_{yz}$ and π^* forms bonding orbital so that it has lower energy than 113β orbital. Both 114α and 114β orbitals are almost same to the π^* orbitals of BL and have anti-bonding character between metals and BL. Similar to the frontier orbitals of **py** complex, those of **bpy** complexes are also constructed from $4d_{yz}$ and $4d_{x^2-y^2}$ orbitals of Ru atoms and π^* orbital of BL. However, contribution of BL $\pi*$ orbital to 132β orbital in **bpy** complex is smaller than that of BL $\pi*$ orbital to 112β orbital in **py** complex. Orbitals of Fe and Os complexes are not shown here but

are qualitatively same to those of Ru complexes. 3*d* and 5*d* orbitals contribute to frontier MOs of Fe and Os complexes, respectively.

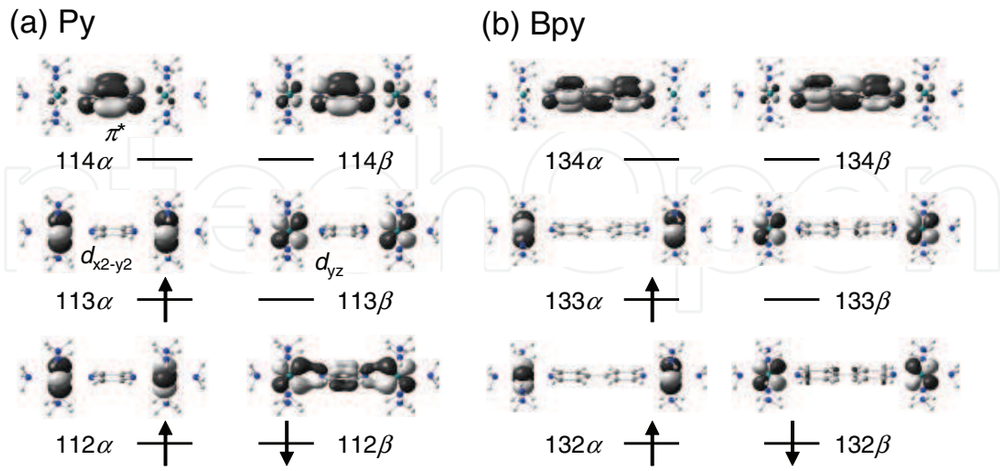


Fig. 5. Frontier molecular orbitals of (a) **py** and (b) **bpy** complexes without input charge.

4. Signal transmission

4.1 Input position

The relation between input position and signal transmission behavior is discussed. About Ru complexes with 5+ charge, switch position $r_{q-\mathrm{Ru}}$ is changed from 5 Å to 15 Å. Input charge is switched from q^{i}=+0.5 to q^{f}=-0.5.

4.1.1 Ru-py complexes

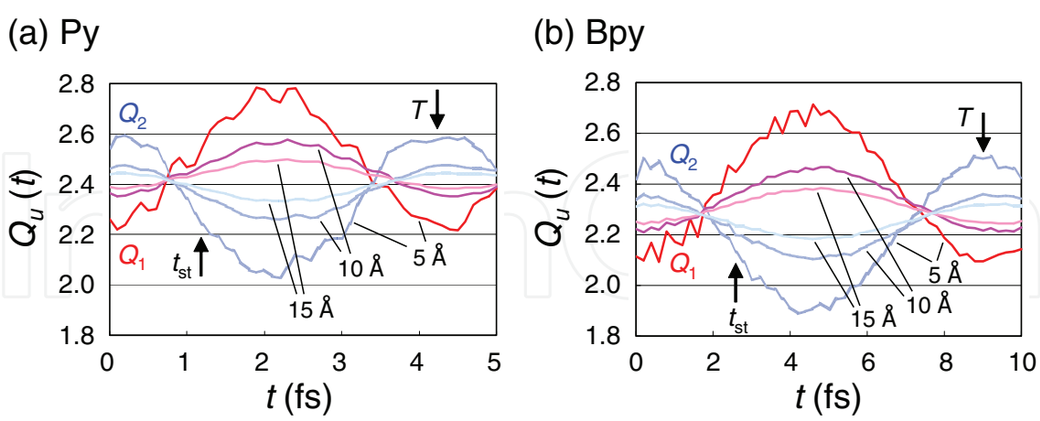


Fig. 6. Dependence of dynamic behavior on input position. Results of (a) **py** and (b) **bpy** complexes.

Figure 6 shows time-evolution of $Q_1(t)$ and $Q_2(t)$ after the switch of the input. The moment of the switch of input corresponds to t=0. Summation of Q_1, Q_2, and charge of LB is always exactly +5. Time evolution of the charge of BL is very small so that is not shown here. As time

flows after the switch, Q_2 decreases and Q_1 increases, namely, signal (electron) is transmitted from U1 to U2 by the Coulombic repulsion.
In **py** results shown in Fig. 6(a), Q_1 becomes almost same to Q_2 at $t \approx 0.8$ fs. At $t \approx 1.2$ fs, Q_1 becomes almost same to $Q_2(0)$, and Q_2 becomes almost same to $Q_1(0)$. Signal transmission is completed at this time, so that the signal transmission time ($t_{\rm st}$) is estimated as $t_{\rm st} \approx 1.2$ fs. After the signal transmission, periodic behavior is repeated with a period of $T \approx 4.3$ fs.
As a whole, the amplitude of the time evolution (signal amplitude: A) is strongly dependent on $r_{q-\rm Ru}$, on the other hand, signal transmission time ($t_{\rm st}$) and period of the evolution (signal period: T) are almost independent of $r_{q-\rm Ru}$. Charge of BL remains almost constant throughout the time evolution, so that signal transmission is said to occur via a hopping mechanism (26). When $r_{q-\rm Ru}$=5 Å, dynamic behavior is a little complicated because that electric field originated from q is so strong that electronic structure is strongly perturbed.

4.1.2 Ru-bpy complexes

Fig. 6(b) shows time-evolution of $Q_1(t)$ and $Q_2(t)$ after the switch of the input. Charge of BL (not shown) remains almost constant throughout the time evolution, so that signal transmission is said to occur via a hopping mechanism as **py** complex. At $t \approx 1.8$ fs, Q_1 and Q_2 become almost the same. At $t \approx 2.6$ fs, Q_1 becomes almost same to $Q_2(0)$, and Q_2 becomes almost same to $Q_1(0)$, so that the signal transmission time is estimated as $t_{\rm st} \approx 2.6$ fs. Periodic behavior is repeated with $T \approx 9.1$ fs. A is strongly dependent on $r_{q-\rm Ru}$, but $t_{\rm st}$ and T are almost independent of $r_{q-\rm Ru}$. It should be noted that A of **bpy** complex is a little larger than that of **py** complex, and $t_{\rm st}$ and T of **bpy** complex are about twice as large as those of **py** complex. Thus, signal transmission through **bpy** complex with long BL is slower than that through **py** complex with short BL. From the viewpoint of signal amplitude, **bpy** complex is better suited for molecular QCA, but from the viewpoint of signal transmission time, dynamic calculation gives the opposite result. This means that for the simulation and design of molecular QCA, dynamic consideration is indispensable.
Signal transmission time $t_{\rm st}$ is 1-2 fs at the maximum. On the other hand, the period T of nuclear motion is usually several tens - several hundreds fs. Therefore, nuclear vibration will have only a small influence on the signal transmission and can be neglected.

4.1.3 Analysis from molecular orbitals (MOs)

It was found that signal amplitude (A) is strongly dependent on $r_{q-\rm Ru}$, on the other hand, signal transmission time ($t_{\rm st}$) and signal period (T) are almost independent of $r_{q-\rm Ru}$. Here, these points are discussed from the viewpoint of MOs and orbitals energies.

4.1.3.1 Molecular orbitals

Figures 7 and 8 show frontier MOs and orbital energies of stationary states of **py** and **bpy** complexes before (q=$q^{\rm i}$) and after (q=$q^{\rm f}$) the switch of the input when $n = 5$.
For **py** complex (Fig. 7), 112α and 113α orbitals dramatically change before and after the switch. Two d_{zx} orbitals, 112α of (a) and 112α of (b), are originally degenerated when q=0.0. This is also applied to a set of 113α of Fig. 7 (a) and 113α of Fig. 7 (b). When q=+0.5, one of two orbitals in which U1 has large distribution is stable due to the Coulombic attraction to the positive q. Inversely, when q=−0.5, the other orbital in which U2 has larger distribution is stable due to the Coulombic repulsion to the negative q. 112β and 113β are almost same to the 112β and 113β orbitals without input charge shown in Fig.5 and are constructed mainly from a linear combination of two 4d_{yz} orbitals of two Ru atoms, one bonding and the other anti-bonding. 112β has larger distribution on U1 when q=+0.5 and on U2 when q=−0.5 due

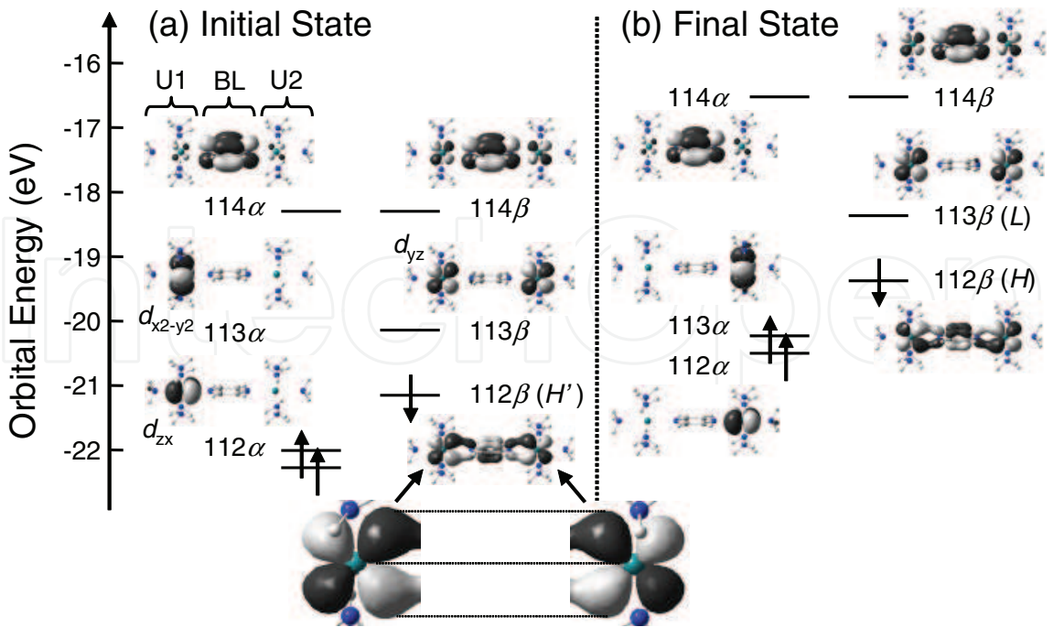


Fig. 7. Frontier molecular orbitals and orbital energies of **py** complex when $n = 5$. (a) *Initial* stationary state ($|\psi^{\mathrm{i}}\rangle$) with q=q^{i}=+0.5 and (b) *final* stationary state ($|\psi^{\mathrm{f}}\rangle$) with q=q^{f}=−0.5. In this figure, input q is placed at a distance of $r_{q-\mathrm{Ru}}$=10Å on the left of the complexes (also see Fig. 4).

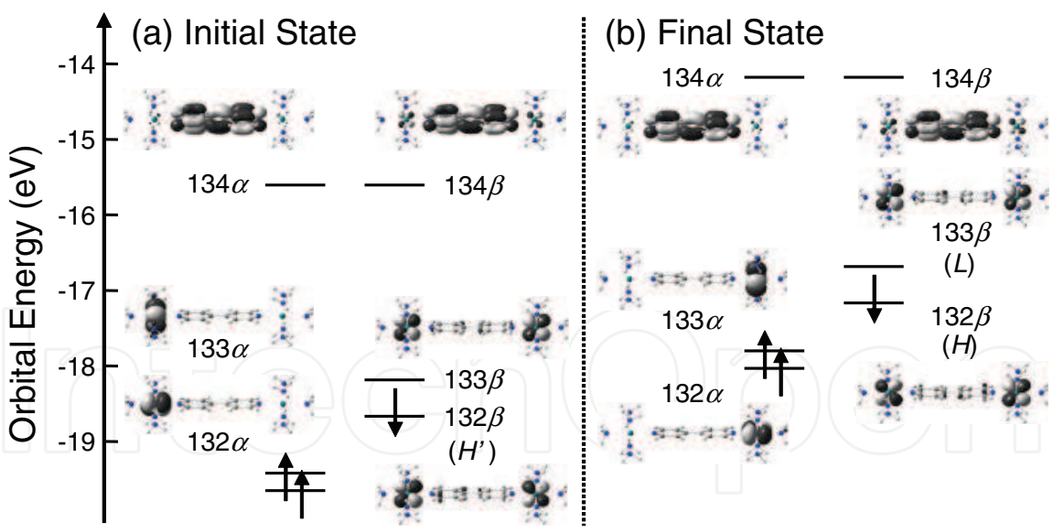


Fig. 8. Frontier molecular orbitals and orbital energies of **bpy** complex when $n = 5$. (a) *Initial* stationary state ($|\psi^{\mathrm{i}}\rangle$) with q=q^{i}=+0.5 and (b) *final* stationary state ($|\psi^{\mathrm{f}}\rangle$) with q=q^{f}=−0.5.

to the Coulombic interaction to the input (see enlarged figures in Fig. 7). However, 113β has opposite character, that is larger distribution on U2 when q=+0.5 and on U1 when q=−0.5, because 112β and 113β are a pair of bonding and anti-bonding orbitals. Larger distribution on one unit of 112β naturally results in smaller distribution on the same unit of 113β.

The same interpretation can be applied to results of **bpy** complex in Fig. 8. 132α and 133α are localized on U1 when q=+0.5 and are localized on U2 when q=−0.5 due to Coulombic interaction. 132β and 133β have bonding and anti-bonding character, respectively, and are mainly constructed from two 4d_{yz} orbitals.

4.1.3.2 Signal period (T)

Time-dependent part of Equation 11 is extracted as

$$\sum_{j,j'\neq j}^{\text{all}} -A_{ujj'}\cos(2\pi t/T_{jj'}), \tag{12}$$

where

$$T_{jj'} = 2\pi/\Delta\varepsilon_{jj'}, \tag{13}$$

$$A_{ujj'} = \sum_{a\in u}^{\text{Atom}}\sum_{\nu\in a}^{\text{Basis}}\sum_{\mu}^{\text{all}}\sum_{n}^{\text{occ.}} d_{jn}d_{j'n}\cdot c_{j\mu}c_{j'\nu}\cdot s_{\mu\nu}. \tag{14}$$

$T_{jj'}$ and $A_{ujj'}$ are the signal period and signal amplitude of unit u of the time evolution, respectively. The term $-A_{ujj'}\cos(2\pi t/T_{jj'})$ represents the contribution of the interaction between $|\psi_j^{\text{f}}\rangle$ and $|\psi_{j'}^{\text{f}}\rangle$ to the time evolution of $Q_u(t)$. All terms with $j = j'$ are excluded because they are time-independent ($\Delta\varepsilon_{jj'} = 0$). In Table 2, two values of $T_{jj'}$ are tabulated in order of $|A_{ujj'}|$. For both **py** and **bpy** complexes, (j, j')=(H, L) term is dominant in U1 and U2 so that the transmission character is almost determined by H and L, where H and L denote HOMO(β) and LUMO(β) of the *final* stationary state (q=q^{f}=−0.5). The values of the second largest $A_{ujj'}$ are negligibly small. Thus, consideration of only (H, L) term is enough to reproduce Fig. 6.
The $T_{jj'}$ (or $\Delta\varepsilon_{jj'}$) with the largest $A_{ujj'}$ mainly determines the period (T) of the time evolution. $T_{jj'}$ is almost independent of $r_{q-\text{Ru}}$ because orbital energies ε_j^{f} are influenced by the strength of electric field originated from the input but energy gaps $\Delta\varepsilon_{jj'}$ between frontier MOs are almost determined by the interaction between Ru atoms, bridging ligand, and ligands, and are little influenced by the strength of electric field originated from the input (see orbitals energies of Figs. 7 and 8).

4.1.3.3 Signal amplitude (A)

In dynamic behavior, signal amplitude (A) is almost determined by the value of A_{uHL}. A_{uHL} is divided into two terms as

$$A_{uHL} = C_{uHL}D_{HL}, \tag{15}$$

where

$$C_{uHL} = \sum_{a\in u}\sum_{\nu\in a}\sum_{\mu} c_{H\mu}c_{L\nu}s_{\mu\nu}, \tag{16}$$

$$D_{HL} = \sum_{n} d_{Hn}d_{Ln}. \tag{17}$$

Absolute values of A_{uHL}, C_{uHL}, and D_{HL} are tabulated in Table 3. As seen from the time evolution in Fig. 6, A_{uHL} sharply decreases as $r_{q-\text{Ru}}$ increases. C_{uHL} changes only a little as

		Unit 1			Unit 2		
	$r_{q-\mathrm{Ru}}$	j, j'	$A_{1jj'}$	$T_{jj'}$	j, j'	$A_{2jj'}$	$T_{jj'}$
py	5Å	$112\beta, 113\beta$	0.128	4.26	$112\beta, 113\beta$	-0.140	4.26
		$106\alpha, 115\alpha$	0.006	0.57	$111\alpha, 114\alpha$	0.008	1.03
	10Å	$112\beta, 113\beta$	0.052	4.47	$112\beta, 113\beta$	-0.053	4.47
		$112\beta, 114\beta$	0.001	1.47	$109\alpha, 114\alpha$	0.002	0.94
	15Å	$112\beta, 113\beta$	0.027	4.47	$112\beta, 113\beta$	-0.028	4.49
		$109\alpha, 114\alpha$	-0.001	0.92	$109\alpha, 114\alpha$	0.001	0.92
bpy	5Å	$132\beta, 133\beta$	0.143	9.06	$132\beta, 133\beta$	-0.145	9.06
		$123\beta, 135\beta$	0.006	0.53	$131\alpha, 134\alpha$	0.004	1.04
	10Å	$132\beta, 133\beta$	0.061	9.34	$132\beta, 133\beta$	-0.061	9.34
		$114\alpha, 135\alpha$	-0.001	0.44	$131\alpha, 134\alpha$	0.001	0.93
	15Å	$132\beta, 133\beta$	0.033	9.36	$132\beta, 133\beta$	-0.033	9.36
		$114\beta, 135\beta$	0.000	0.43	$130\alpha, 134\alpha$	0.001	0.91

Table 2. Contribution of a set of (j, j') orbitals to the time-evolution of Mulliken charge. Two values of $T_{jj'}$ (fs) are shown in order of $|A_{ujj'}|$ (e). For all complexes, the set of (HOMO(β), LUMO(β)) gives the largest $A_{ujj'}$.

$r_{q-\mathrm{Ru}}$ increases, but D_{HL} sharply decreases as $r_{q-\mathrm{Ru}}$ increases. Thus, the decrease in A_{uHL} attendant on the increase of $r_{q-\mathrm{Ru}}$ is mainly due to the decrease in D_{HL}. Although D_{HL} is defined as a summation over all MOs n as seen in Equation 17, $d_{HH'}d_{LH'}$ among all $d_{Hn}d_{Ln}$ has the dominant contribution to D_{HL}, where H' is HOMO(β) of the *initial* stationary state (q=q^{i}=+0.5), because d_{Hn} is almost zero except for $n = H'$. Additionally, although the values of $d_{HH'}$ are almost constant ($0.926 < d_{HH'} < 0.998$) for all BL and $r_{q-\mathrm{Ru}}$, $d_{LH'}$ is strongly dependent on $r_{q-\mathrm{Ru}}$ as shown in Table 3. As $r_{q-\mathrm{Ru}}$ becomes smaller, the values of $d_{HH'}$ deviate from 1. The values of $d_{LH'}/A_{uHL}$ are almost constant for all $r_{q-\mathrm{Ru}}$. Consequently, we can approximate Equation 15 as

$$|A_{uHL}| \propto |d_{LH'}|. \tag{18}$$

H' and L have been already shown in Figs. 7 and 8. In both complexes, larger distribution of H' is located on U1. Similarly, larger distribution of L is on U1. For both complexes, the function $\psi_L^{\mathrm{f}}\,\psi_{H'}^{\mathrm{i}}$ has positive value around U1 and negative value around U2. $\psi_L^{\mathrm{f}}\,\psi_{H'}^{\mathrm{i}}$ has larger distribution on U1 than on U2, so that the overlap integral $d_{LH'} = \langle\psi_L^{\mathrm{f}}|\psi_{H'}^{\mathrm{i}}\rangle$ has non-zero value in total. If the input is positioned considerably far from the complex (this situation is equivalent to $q^{\mathrm{i}} \approx q^{\mathrm{f}} \approx 0$), the value of $d_{LH'}$ is almost zero because L and H' are almost orthogonal. Namely, the input placed nearer to the molecule leads to more asymmetric H' and L, so that $d_{LH'}$, in other words, A_{uHL} tends to be large. All complexes with **bpy** BL have small coefficients on BL and MOs distribute mainly on the metal atoms. Thus, the distribution of frontier orbitals of **bpy** complexes is strongly influenced by the switch of the input and signal amplitude A of **bpy** complexes is larger than that of py complexes.

4.2 Switch power

The relation between switch power and signal transmission behavior is discussed. Switch power corresponds to the difference between q^{i} and q^{f}. About Ru complexes with $n = 5$ and $r_{q-\mathrm{Ru}} = 10$ Å, three kinds of switch, (q^{i}, q^{f}) = (+0.1, -0.1), (+0.3, -0.3), and (+0.5, -0.5), are simulated.

	py			**bpy**		
$r_{q-\mathrm{Ru}}$	5Å	10Å	15Å	5Å	10Å	15Å
A_{uHL}	0.128	0.052	0.027	0.143	0.061	0.033
C_{uHL}	0.378	0.418	0.424	0.412	0.444	0.448
D_{HL}	0.338	0.125	0.065	0.348	0.137	0.075
$d_{HH'}d_{LH'}$	0.338	0.125	0.065	0.348	0.137	0.075
$d_{HH'}$	0.931	0.992	0.998	0.926	0.990	0.997
$d_{LH'}$	0.364	0.126	0.065	0.376	0.139	0.075
$d_{LH'}/A_{uHL}$	2.84	2.42	2.41	2.63	2.28	2.27

Table 3. Absolute values of A_{uHL}, C_{uHL}, D_{HL}, $d_{HH'}d_{LH'}$, $d_{HH'}$, $d_{LH'}$, and $d_{LH'}/A_{uHL}$ of unit 2.

4.2.1 Ru-py and Ru-bpy complexes

Figure 9(a) shows the results of **py** complex. Signal period (T) is 4.3 fs and signal transmission time (t_{st}) is 1.2 fs, and both are independent of (q^{i}, q^{f}). On the other hand, signal amplitude (A) decreases as (q^{i}, q^{f}) becomes small. This is because that MOs become more symmetric as (q^{i}, q^{f}) becomes small so that values of $d_{LH'}$ becomes small. Figure 9(b) shows the results of **bpy** complex. Signal period (T) is 9.1 fs and signal transmission time (t_{st}) is 2.6 fs. Dependence of A and T on the switch power is same to the result of **py** complex.

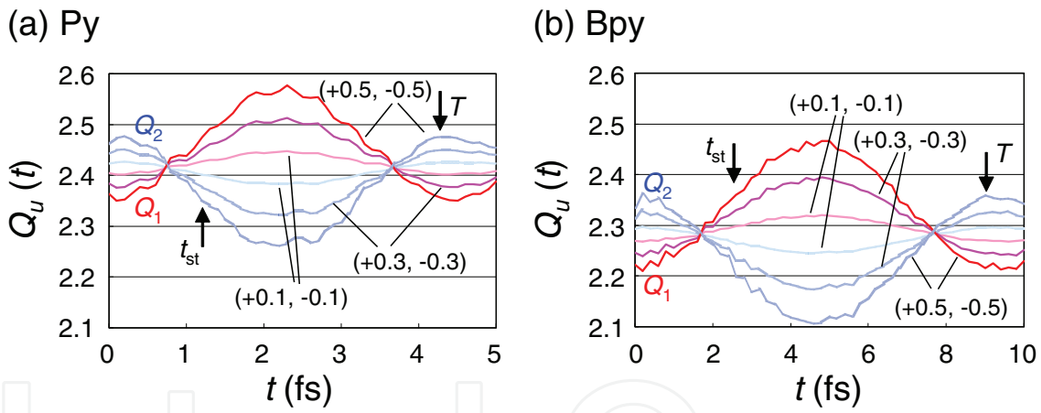


Fig. 9. Dependence of dynamic behavior on switch power. Results of (a) **py** and (b) **bpy** complexes

4.2.2 Analysis from MOs

In Table 4, the largest $|A_{ujj'}|$ and corresponding $T_{jj'}$ are tabulated. Similar to the discussion about the input position, (j, j') = (H, L) term is dominant so that the transmission behavior is almost determined by H and L. The $T_{jj'}$ (or $\Delta\varepsilon_{jj'}$) with the largest $A_{ujj'}$ mainly determines the period (T) of the time evolution of Figure 9.

Absolute values of A_{uHL}, C_{uHL}, and D_{HL} are tabulated in Table 5. We can see that the order of D_{HL} qualitatively correspond to that of A_{uHL}. Therefore, the analysis of D_{HL} is necessary for understanding the values of A_{uHL}. $d_{HH'}d_{LH'}$ term among all $d_{Hn}d_{Ln}$ terms has the dominant contribution to D_{HL}. Although the values of $d_{HH'}$ are almost an unit ($0.990 < d_{HH'} < 1.000$) for all complexes, $d_{LH'}$ is strongly dependent on the switch power.

		Unit 1			Unit 2		
	$(q^{\mathrm{i}}, q^{\mathrm{f}})$	j, j'	$A_{1jj'}$	$T_{jj'}$	j, j'	$A_{2jj'}$	$T_{jj'}$
py	(+0.1,-0.1)	$112\beta, 113\beta$	0.011	4.50	$112\beta, 113\beta$	-0.011	4.50
	(+0.3,-0.3)	$112\beta, 113\beta$	0.032	4.49	$112\beta, 113\beta$	-0.032	4.49
	(+0.5,-0.5)	$112\beta, 113\beta$	0.052	4.47	$112\beta, 113\beta$	-0.053	4.47
bpy	(+0.1,-0.1)	$132\beta, 133\beta$	0.012	9.37	$132\beta, 133\beta$	-0.012	9.37
	(+0.3,-0.3)	$132\beta, 133\beta$	0.037	9.36	$132\beta, 133\beta$	-0.037	9.36
	(+0.5,-0.5)	$132\beta, 133\beta$	0.061	9.34	$132\beta, 133\beta$	-0.061	9.34

Table 4. Dependence of dynamic parameters, $|A_{ujj'}|$ and $T_{jj'}$, on switch power.

Consequently, we can qualitatively discuss the values of $|A_{uHL}|$ from those of $|d_{LH'}|$. As the switch power increases, asymmetry of H' and L increases. Therefore, signal amplitude A also increase. These discussions about switch power are qualitatively same to those of input position in the subsection 4.1. Thus, a decrease in $(q^{\mathrm{i}}, q^{\mathrm{f}})$ is equivalent to an increase in $r_{q-\mathrm{Ru}}$.

	py			**bpy**		
$(q^{\mathrm{i}}, q^{\mathrm{f}})$	(+0.1,-0.1)	(+0.3,-0.3)	(+0.5,-0.5)	(+0.1,-0.1)	(+0.3,-0.3)	(+0.5,-0.5)
A_{uHL}	0.011	0.032	0.053	0.012	0.037	0.061
C_{uHL}	0.429	0.429	0.429	0.449	0.448	0.445
D_{HL}	0.025	0.075	0.125	0.028	0.083	0.137
$d_{HH'}d_{LH'}$	0.025	0.075	0.125	0.028	0.083	0.137
$d_{HH'}$	1.000	0.997	0.995	1.000	0.997	0.990
$d_{LH'}$	0.025	0.075	0.126	0.028	0.083	0.139
$d_{LH'}/A_{uHL}$	2.27	2.34	2.38	2.33	2.24	2.28

Table 5. Absolute values of A_{uHL}, C_{uHL}, D_{HL}, $d_{HH'}d_{LH'}$, $d_{HH'}$, $d_{LH'}$, and $d_{LH'}/A_{uHL}$ of U2.

4.3 Complex charge

The relation between complex charge and signal transmission behavior is discussed about Ru complexes. Complex charge $n+$ is set at 4+, 5+, and 6+. Electronic structures of complexes with $n+ = 4+, 6+$ charges were obtained by the single point calculations of the complex with the optimized geometry in $n+ = 5+$ charged state. Complex with 5+ charge is open-shell systems, and those with 4+ and 6+ are closed-shell system. In the calculation, other parameters are fixed at $r_{q-\mathrm{Ru}} = 10$Å and $(q^{\mathrm{i}}, q^{\mathrm{f}})$=(+0.5, -0.5).

4.3.1 Ru-py and Ru-bpy complexes

Figure 10(a) shows time evolution of $Q_1(t)$ and $Q_2(t)$ of **py** complexes with 4+, 5+, and 6+ charges. Signal transmission time t_{st} is estimated as 0.3 fs (4+) $<$ 1.2 fs (5+) $<$ 1.5 fs (6+) and values of signal amplitude A are estimated as 0.01 e (6+) $<$ 0.02 e (4+) $<$ 0.05 e (5+). After the signal transmission, periodic behavior is repeated with a period (T) of 1.5 fs (4+) $<$ 4.5 fs (5+) $<$ 5.7 fs (6+). From the viewpoint of operation speed of QCA device, 4+ complex is most useful. On the other hand, from the viewpoint of signal amplitude of QCA device, 5+ complex is most useful.

Figure 10(b) shows time evolution of $Q_1(t)$ and $Q_2(t)$ of **bpy** complexes. Signal transmission time t_{st}, signal amplitude A, and signal period T are estimated as 0.2 fs (4+) $<$ 2.2 fs (5+) $\approx$

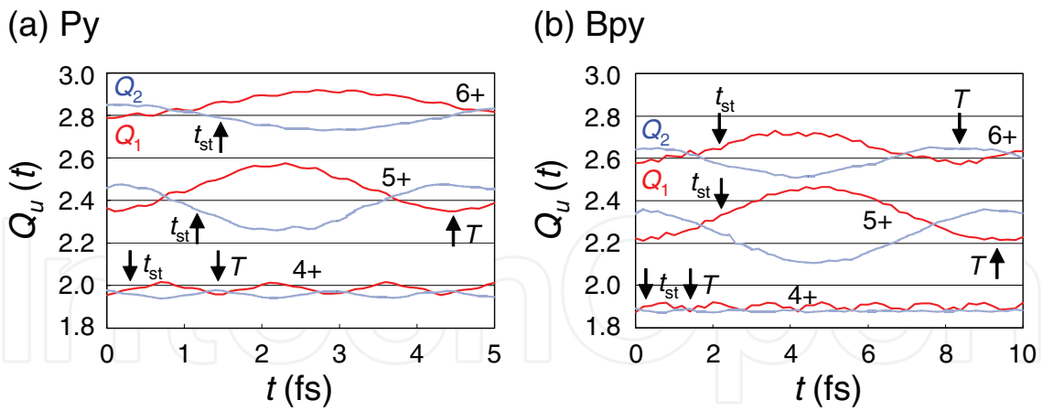


Fig. 10. Dependence of dynamic behavior on complex charge. Results of (a) **py** and (b) **bpy** complexes

2.2 fs (6+), 0.01 e (4+) < 0.02 e (6+) < 0.06 e (5+), and 1.4 fs (4+) < 8.3 fs (6+) < 9.3 fs (5+), respectively. From the viewpoint of operation speed of QCA device, 4+ complex is most useful. On the other hand, from the viewpoint of signal power of QCA device, 5+ complex is most useful. This result is qualitatively same to the results of **py** complex.

4.3.2 Analysis from MOs

Figures 11 and 12 show frontier MOs and orbital energies of stationary states of **py** and **bpy** complexes before and after the switch of the input. Only HOMO and LUMO are shown here since other orbitals play almost no role in signal transmission (24). These MOs are almost same to the orbitals shown in Fig. 5. However, LUMO of 6+ complexes are different between *initial* and *final* stationary states for **py** and **bpy** complex.

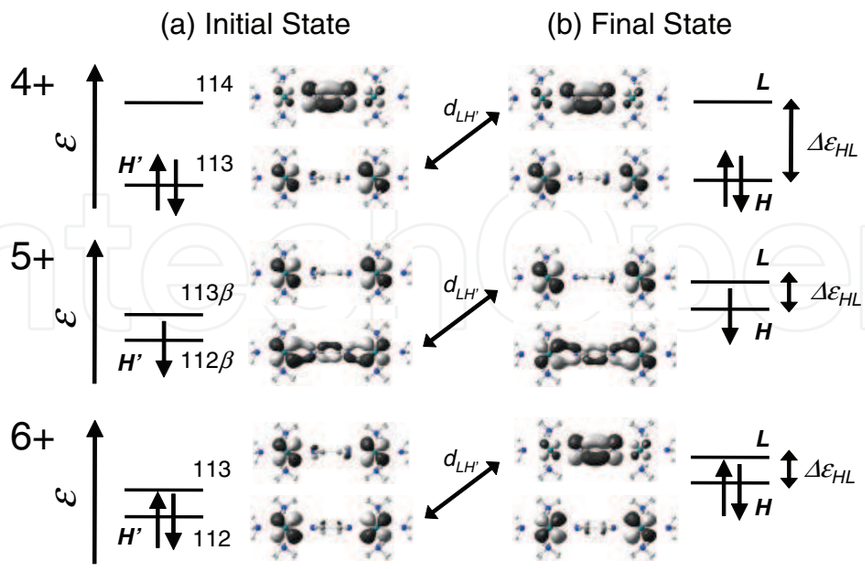


Fig. 11. Frontier molecular orbitals and orbital energies of **py** complex. (a) *Initial* stationary state ($|\psi^{i}\rangle$) with q=q^{i}=+0.5 and (b) *final* stationary state ($|\psi^{f}\rangle$) with q=q^{f}=−0.5.

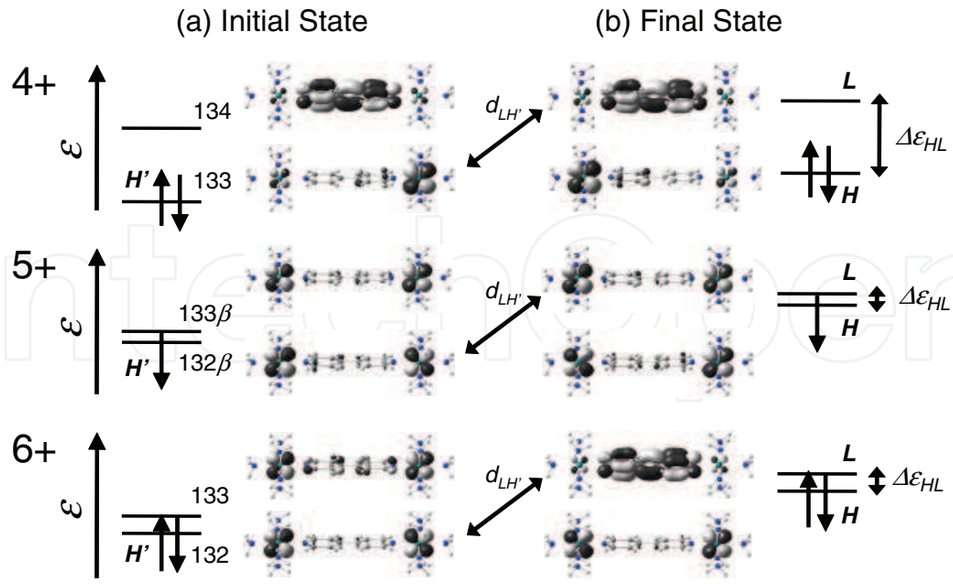


Fig. 12. Frontier molecular orbitals and orbital energies of **bpy** complex. (a) *Initial* stationary state ($|\psi^{\mathrm{i}}\rangle$) with q=q^{i}=+0.5 and (b) *final* stationary state ($|\psi^{\mathrm{f}}\rangle$) with q=q^{f}=−0.5.

In Table 6, two values of $T_{jj'}$ are tabulated in order of $|A_{ujj'}|$. Except for **bpy** complex with 4+ charge, $(j, j') = (H, L)$ term is dominant so that the transmission behavior is almost determined by H and L except for **bpy** complex with 4+ charge. The $T_{jj'}$ (or $\Delta\varepsilon_{jj'}$) with the largest $A_{ujj'}$ mainly determines the period (T) of the time evolution of Figure 10. H-L energy gap (ε_{HL}) of 4+ complexes is very large so that signal period T is very short.

		Unit 1			Unit 2		
	n+	j, j'	$A_{1jj'}$	$T_{jj'}$	j, j'	$A_{2jj'}$	$T_{jj'}$
py	4+	113, 114	0.005	1.45	113, 114	-0.004	1.35
		106, 119	0.001	0.48	101, 117	0.000	0.45
	5+	112β, 113β	0.052	4.47	112β, 113β	-0.053	4.47
		112β, 114β	0.001	1.47	109α, 114α	0.002	0.94
	6+	112, 113	0.015	5.74	112, 113	-0.015	5.74
		102, 115	0.001	0.58	101, 116	-0.001	0.53
bpy	4+	133, 134	0.003	1.36	130, 134	-0.001	1.24
		124, 143	0.002	0.47	133, 134	-0.001	1.36
	5+	132β, 133β	0.061	9.34	132β, 133β	-0.061	9.34
		114α, 135α	-0.001	0.44	131α, 134α	0.001	0.93
	6+	132, 133	0.017	8.29	132, 133	-0.017	8.29
		125, 133	0.002	2.11	125, 133	0.002	2.11

Table 6. Dependence of dynamics parameters, $|A_{ujj'}|$ and $T_{jj'}$, on complex charge.

Absolute values of A_{uHL}, C_{uHL}, and D_{HL} are tabulated in Table 7. In previous sections, the values of $|A_{uHL}|$ were proportional to those of $|d_{LH'}|$ since the values of C_{uHL} were almost constant for all cases (24). In this section, however, the values of $|A_{uHL}|$ are not exactly proportional to those of $|d_{LH'}|$ since the values of C_{uHL} also depend on the number of occupied

orbitals. We can see that the order of D_{HL} qualitatively corresponds to that of $d_{LH'}$. 4+ and 6+ complexes have much smaller $d_{LH'}$ than 5+ complexes. This is because that 4+ and 6+ complexes have closed-shell electronic structures, therefore, input switch has little influence on the shapes of H' and L. On the other hand, 5+ complexes have open-shell electronic structures, so that the molecular orbital is sensitive to the input charge. These results mean that mixed-valence complexes are suitable for QCA application.

	py			**bpy**		
n+	4+	5+	6+	4+	5+	6+
A_{uHL}	0.004	0.053	0.015	0.001	0.061	0.017
C_{uHL}	0.122	0.429	0.461	0.037	0.445	0.428
D_{HL}	0.029	0.125	0.033	0.023	0.137	0.039
$d_{HH'}d_{LH'}$	0.025	0.088	0.033	0.009	0.137	0.039
$d_{HH'}$	0.926	0.996	0.999	0.497	0.990	0.999
$d_{LH'}$	0.027	0.088	0.033	0.018	0.139	0.039

Table 7. Absolute values of A_{uHL}, C_{uHL}, D_{HL}, $d_{HH'}d_{LH'}$, $d_{HH'}$, and $d_{LH'}$ of U2

4.4 Kind of metals

The relation between metal atoms and signal transmission behavior is discussed. Metal is changed Fe, Ru, and Os. Complex charge and switch power are selected as 5+ and (+0.5, -0.5), respectively.

4.4.1 M-py and M-bpy complexes

Figure 13(a) shows time evolution of $Q_1(t)$ and $Q_2(t)$ of **py** complexes after the switch of the input from $q = +0.5$ to $q = -0.5$. Signal transmission time t_{st} is estimated as 0.6 fs (Fe) $<$ 0.7 fs (Os) $<$ 1.1 fs (Ru). After the signal transmission, periodic behavior is repeated with a period (T) of 2.0 fs (Fe) $<$ 2.5 fs (Os) $<$ 4.5 fs (Ru). From the Figures, values of signal amplitude A are estimated as 0.05 e (Fe) $<$ 0.06 e (Os) $<$ 0.10 e (Ru). All t_{st}, T, and A are dependent on the kind of metal. From the viewpoint of operation speed of QCA device, Fe complex is most useful. On the other hand, from the viewpoint of signal power of QCA device, Ru complex is most useful.

Figure 13(b) shows time-evolution of $Q_1(t)$ and $Q_2(t)$ of **bpy** complexes. Signal transmission time t_{st} is estimated as 1.4 fs (Fe) $<$ 1.7 fs (Os) $<$ 2.5 fs (Ru). After the signal transmission, periodic behavior is repeated with a period (T) of 5.2 fs (Fe) $<$ 6.3 fs (Os) $<$ 9.3 fs (Ru). These values of T are almost twice as large as those of **py** complexes, and are valid considering the difference in molecular size between **py** and **bpy** bridging ligands. The values of A are estimated as 0.11 e (Os) $<$ 0.12 e (Ru) $<$ 0.13 e (Fe). From the viewpoints of both operation speed and signal power of QCA device, Fe complex shows good result.

4.4.2 Analysis from MO

Figures 14 and 15 show frontier MOs and orbital energies of stationary states of **py** and **bpy** complexes before (a) and after (b) the switch of the input. Only HOMO and LUMO with β spin are shown here since other orbitals play almost no role in signal transmission (24). These MOs are mainly constructed from π^* orbital of BL and d_{yz} orbital of M atom. HOMOs have larger distribution on U1 when $q = +0.5$ e due to the Coulombic attraction. On the other hand, when $q = -0.5$ e, HOMOs have smaller distribution on U1 due to the Coulombic repulsion.

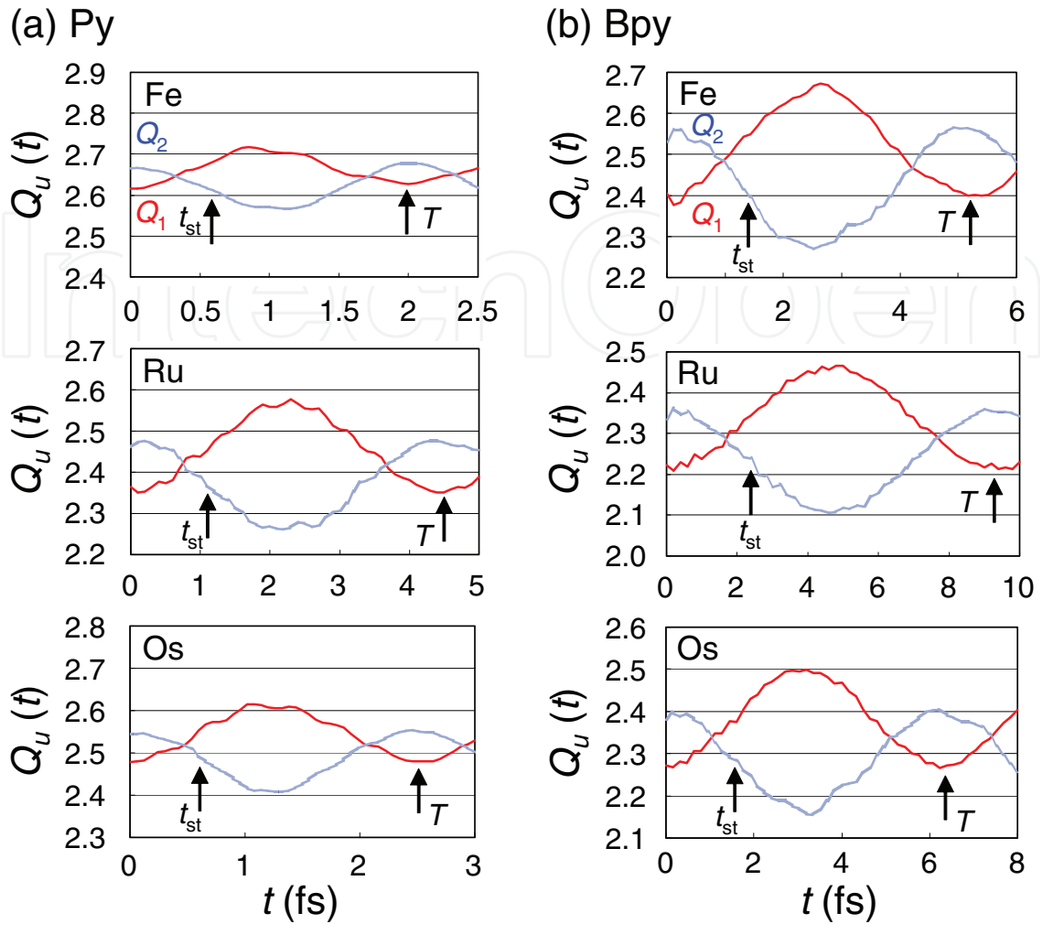


Fig. 13. Dependence of dynamic behavior on metal atoms. Results of (a) **py** and (b) **bpy** complexes.

In Table 8, the largest $|A_{ujj'}|$ and corresponding value of $T_{jj'}$ are tabulated. For all complexes, $(j, j') = (H, L)$ term is dominant so that the transmission behavior is almost determined by H and L. The $T_{jj'}$ (or $\Delta\varepsilon_{jj'}$) with the largest $A_{ujj'}$ mainly determine the period (T) of the time evolution of Figure 13. Orbital energies $\varepsilon_j^{\mathrm{f}}$ are influenced by the strength of electric field originated from the input, but energy gaps $\Delta\varepsilon_{jj'}$ between frontier MOs are almost determined by the interaction between metal atoms, bridging ligand, and ligands. Difference in the kind of metal atoms results in the difference in this interaction ($\Delta\varepsilon_{jj'}$ and $T_{jj'}$).
Absolute values of A_{uHL}, C_{uHL}, and D_{HL} are tabulated in Table 9. We can see that the order of D_{HL} qualitatively correspond to that of A_{uHL}. Therefore, the analysis of D_{HL} is necessary for understanding the values of A_{uHL}. $d_{HH'}d_{LH'}$ term among all $d_{Hn}d_{Ln}$ terms has the dominant contribution to D_{HL}. Additionally, although the values of $d_{HH'}$ are almost an unit ($0.980 < d_{HH'} < 0.996$) for all complexes, $d_{LH'}$ is strongly dependent on the kind of metal. Consequently, we can qualitatively discuss the values of $|A_{uHL}|$ from that of $|d_{LH'}|$. H' and L have been already shown in Figures 14 and 15. The values of $|A_{uHL}|$ are not exactly proportional to those of $|d_{LH'}|$ since the values of C_{uHL} also depend on the kind of metal atoms. In all complexes, larger distribution of H' is located on U1 (left-hand side). Similarly,

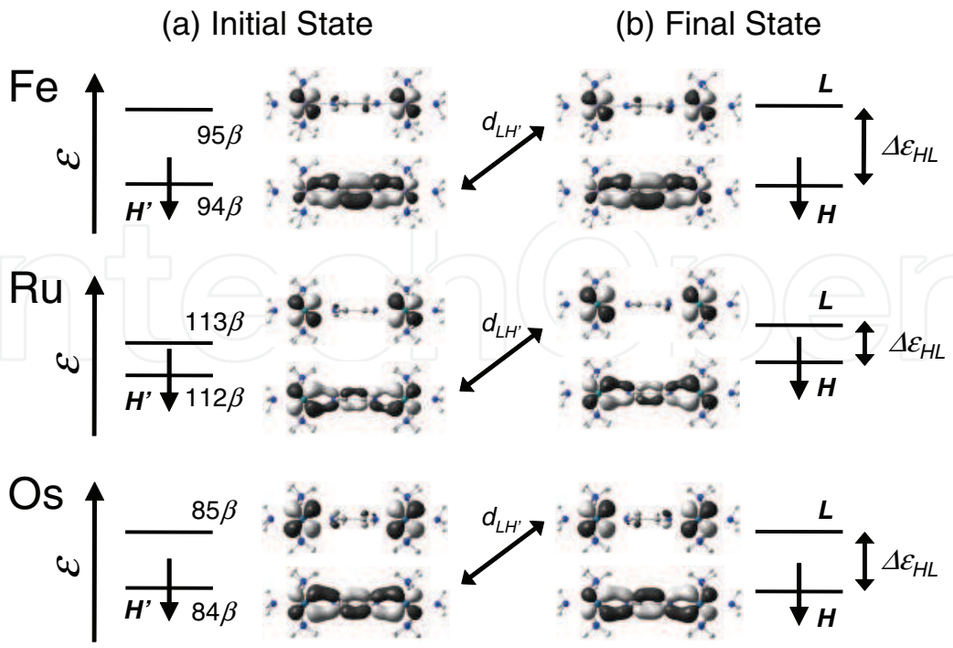


Fig. 14. Frontier molecular orbitals and orbital energies of **py** complex. (a) *Initial* stationary state ($|\psi^{\mathrm{i}}\rangle$) with q=q^{i}=+0.5 and (b) *final* stationary state ($|\psi^{\mathrm{f}}\rangle$) with q=q^{f}=−0.5.

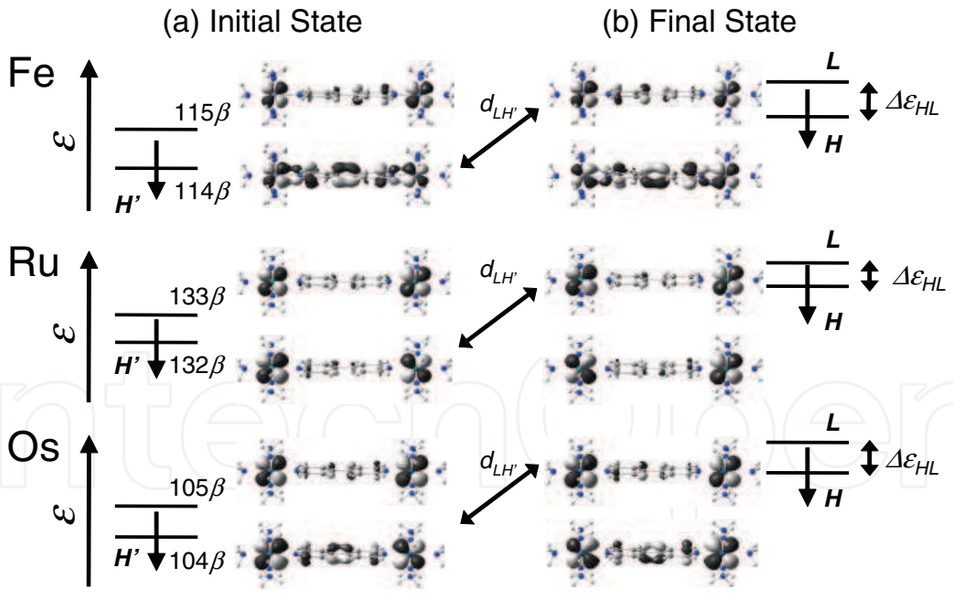


Fig. 15. Frontier molecular orbitals and orbital energies of **bpy** complex. (a) *Initial* stationary state ($|\psi^{\mathrm{i}}\rangle$) with q=q^{i}=+0.5 and (b) *final* stationary state ($|\psi^{\mathrm{f}}\rangle$) with q=q^{f}=−0.5.

larger distribution of L is on U1. For all complexes, $\psi_L^{\mathrm{f}}\,\psi_{H'}^{\mathrm{i}}$ has larger distribution on U1 than on U2, so that the overlap integral $d_{LH'} = \langle\psi_L^{\mathrm{f}}|\psi_{H'}^{\mathrm{i}}\rangle$ has non-zero value in total.
About **py** complexes, H' and L of Ru complex have large distribution on the Ru metal but those of Fe complex have small distribution on the Fe metal from Figure 7. Therefore,

		Unit 1			Unit 2		
	M	j, j'	$A_{1jj'}$	$T_{jj'}$	j, j'	$A_{2jj'}$	$T_{jj'}$
py	Fe	$94\beta, 95\beta$	0.021	2.00	$94\beta, 95\beta$	-0.026	2.00
	Ru	$112\beta, 113\beta$	0.052	4.47	$112\beta, 113\beta$	-0.053	4.47
	Os	$84\beta, 85\beta$	0.031	2.48	$84\beta, 85\beta$	-0.033	2.48
bpy	Fe	$114\beta, 115\beta$	0.065	5.15	$114\beta, 115\beta$	-0.071	5.15
	Ru	$132\beta, 133\beta$	0.061	9.34	$132\beta, 133\beta$	-0.061	9.34
	Os	$104\beta, 105\beta$	0.056	6.26	$104\beta, 105\beta$	-0.057	6.26

Table 8. Dependence of dynamics parameters, $|A_{ujj'}|$ and $T_{jj'}$, on kind of metals.

	py			**bpy**		
M	Fe	Ru	Os	Fe	Ru	Os
A_{uHL}	0.026	0.053	0.033	0.071	0.061	0.057
C_{uHL}	0.295	0.429	0.352	0.372	0.445	0.401
D_{HL}	0.088	0.125	0.093	0.192	0.137	0.141
$d_{HH'}d_{LH'}$	0.088	0.125	0.093	0.192	0.137	0.141
$d_{HH'}$	0.996	0.992	0.996	0.980	0.990	0.990
$d_{LH'}$	0.088	0.126	0.094	0.195	0.139	0.143

Table 9. Absolute values of A_{uHL}, C_{uHL}, D_{HL}, $d_{HH'}d_{LH'}$, $d_{HH'}$, and $d_{LH'}$ of U2.

the distribution of frontier orbitals of Ru complexes is strongly influenced by the switch of the input. Consequently, strongly deformed H' and L give large $d_{LH'}$ and A. About **bpy** complexes, simple interpretation like **py** complexes are a little difficult because the difference in MO coefficients between metals of **bpy** complexes is smaller than that of **py** complexes. All complexes with **bpy** BL have small coefficients on BL and MOs distribute mainly on the metal atoms. Thus, signal amplitude A of **bpy** complexes is larger than that of **py** complexes and the difference in A between **bpy** complexes is small.

5. Summary

With a view to analysing the dynamic behavior of molecular QCA device and designing molecular QCA candidate, a new theoretical approach from frontier molecular orbitals are discussed. From the detailed analysis of the dynamic behavior based on MOs and orbital energies, the following three general points were found:

- Signal amplitude (A) through the complexes strongly depends on (q^{i}, q^{f}) and $r_{q-\mathrm{M}}$, and its magnitude is explained from the asymmetry of MOs due to the input charge and the overlap between MOs.
- Signal period (T) is independent of (q^{i}, q^{f}) and $r_{q-\mathrm{M}}$ because T is determined from energy gaps between MOs ($\Delta\varepsilon$) which is independent of (q^{i}, q^{f}) and $r_{q-\mathrm{M}}$.
- Signal transmission time (t_{st}) is determined depending on the balance of A and T.

For dinuclear complexes discussed in this Chapter, discussions mainly about $d_{LH'}$ and $\Delta\varepsilon_{HL}$ are valid except for only one system, **bpy** complex with 4+ charge. These results could be useful guidelines for molecular design of molecular QCA candidates. Generally, Class III

complexes with large A (large overlap) and small T (large $\Delta\varepsilon$) tend to give small t_{st}, and could be good molecular QCA candidates.
This analysis method was applied to many varieties of QCA pattern, input position, switch power, complex charge, and kind of metals, and we found that

- **bpy** complexes generally have stronger signal amplitude (A), but waste longer time (t_{st}) for signal transmission than **py** complexes
- Strong switch power (q^i, q^f) results in the large signal amplitude (A). Change in switch power corresponds to the change in input position (r_{q-M}).
- MOs of mixed-valence complexes ($n = 5$) are sensitive to the change in input charge q. Thus, these complexes are suitable for molecular QCA from the viewpoint of signal amplitude (A).
- Large MO coefficient on metal atoms leads to the large A since shapes of such MOs are greatly influenced by the switch.

Lastly, it should be noted that these method can be easily applied to the reverse switch (24). Results by HF method can be discussed similarly, but signal transmission is difficult to occur since HF method tends to overestimate the electron localization.

6. Acknowledgements

Theoretical research shown in this Chapter was supported by the Joint Studies Program (2010) of the Institute for Molecular Science (IMS). The author would like to thank Dr. Hiroshi Kawabata of Hiroshima University for helpful comments to this chapter. Theoretical calculations were mainly carried out using the computer facilities at Research Center for Computational Science (Okazaki, Japan) and Research Institute for Information Technology, Kyushu University (Fukuoka, Japan).

7. References

[1] Zhirnov, V.V.; Hutchby, J.A.; Bourianoff, G.I.; Brewer, J.E. Emerging research logic devices. An assessment of new field-effect transistor, resonant tunnel device, single-electron transistor, and quantum cellular automata technologies. *IEEE Circ. Dev. Mag.* 2005, *21*, 37–46.
[2] Lent, C.S.; Tougaw, P.D.; Porod, W.; Bernstein, G.H. Quantum cellular automata. *Nanotechnology* 1993, *4*, 49–57.
[3] Orlov, A.O.; Amlani, I.; Berstein, G.H.; Lent, C.S.; Snider, G.L. Realization of a functional cell for quantum-dot cellular automata. *Science* 1997, *277*, 928–930.
[4] Amlani, I.; Orlov, A.O.; Toth, G.; Berstein, G.H.; Lent, C.S.; Snider, G.L. Digital logic gate using quantum-dot cellular automata. *Science* 1999, *284*, 289–291.
[5] Lent, C.S. Molecular electronics: Bypassing the transistor paradigm. *Science* 2000, *288*, 1597–1599.
[6] Lau, V.C.; Berben, L.A.; Long, J.R. $[(Cyclen)_4Ru_4(pz)_4]^{9+}$: A Creutz-Taube square. *J. Am. Chem. Soc.* 2002, *124*, 9042–9043.
[7] Yao, H.; Sabat, M.; Grimes, R.N.; de Biani, F.F.; Zanello, P. Metallacarborane-based nanostructures: A carbon-wired planar cctagon. *Angew. Chem. Int. Ed.* 2003, *42*, 1002–1005.

[8] Jiao, J.; Long, G.J.; Grandjean, F.; Beatty, A.M.; Fehlner, T.P. Building blocks for the molecular expression of quantum cellular automata. Isolation and characterization of a covalently bonded square array of two ferrocenium and two ferrocene complexes. *J. Am. Chem. Soc.* 2003, *125*, 7522–7523.

[9] Jiao, J.; Long, G.J.; Rebbouh, L.; Grandjean, F.; Beatty, A.M.; Fehlner, T.P. Properties of a mixed-valence $(Fe(II))_2(Fe(III))_2$ square cell for utilization in the quantum cellular automata paradigm for molecular electronics. *J. Am. Chem. Soc.* 2005, *127*, 17819–17831.

[10] Berben, L.A.; Faia, M.C.; Crawford, N.R.M.; Long, J.R. Angle dependent electronic effects in 4,4-bipyridine-bridged Ru_3 triangle and Ru_4 square complexes. *Inorg. Chem.* 2006, *45*, 6378–6386.

[11] Qi, H.; Sharma, S.; Li, Z.; Snider, G.L.; Orlov, A.O.; Lent, C.; Fehlner, T.P. Molecular quantum cellular automata cells. Electric field driven switching of a silicon surface bound array of vertically oriented two-dot molecular quantum cellular automata. *J. Am. Chem. Soc.* 2003, *125*, 15250–15259.

[12] Qi, H.; Gupta, A.; Noll, B.C.; Snider, G.L.; Lu, Y.; Lent, C.; Fehlner, T.P. Dependence of field switched ordered arrays of dinuclear mixed-valence complexes on the distance between the redox centers and the size of the counterions. *J. Am. Chem. Soc.* 2005, *127*, 15218–15227.

[13] Wei, Z.; Guo, S.; Kandel, S.A. Observation of single dinuclear metal-complex molecules using scanning tunneling microscopy. *J. Phys. Chem. B* 2006, *110*, 21846–21849.

[14] Manimaran, M.; Snider, G.L.; Lent, C.S.; Sarveswaran, V.; Lieberman, M.; Li, Z.; Fehlner, T.P. Scanning tunneling microscopy and spectroscopy investigations of QCA molecules. *Ultramicroscopy* 2003, *97*, 55–63.

[15] Lu, Y.; Quardokus, R.; Lent, C.S.; Justaud, F.; Lapinte, C.; Kandel, S.A. Charge Localization in Isolated Mixed-Valence Complexes: An STM and Theoretical Study. *J. Am. Chem. Soc. 2010, 132*, 13519-13524

[16] Guo, S.; Kandel, S.A. Scanning Tunneling Microscopy of Mixed Valence Dinuclear Organometallic Cations and Counterions on Au(111). *J. Chem. Phys. Lett. 2010, 1*, 420-424.

[17] Braun-Sand, S.B.; Wiest, O. Theoretical studies of mixed-valence transition metal complexes for molecular computing. *J. Phys. Chem. A* 2003, *107*, 285–291.

[18] Braun-Sand, S.B.; Wiest, O. Biasing mixed-valence transition metal complexes in search of bistable complexes for molecular computing. *J. Phys. Chem. B* 2003, *107*, 9624–9628.

[19] Lent, C.S.; Isaksen, B.; Lieberman, M. Molecular quantum-dot cellular automata. *J. Am. Chem. Soc.* 2003, *125*, 1056–1063.

[20] Lent, C.S.; Isaksen, B. Clocked molecular quantum-dot cellular automata. *IEEE Trans. Electron Devices* 2003, *50*, 1890–1896.

[21] Lu, Y.; Lent, C.S. Theoretical study of molecular quantum-dot cellular automata. *J. Comput. Electron.* 2005, *4*, 115–118.

[22] Timler, J.; Lent, C.S. Maxwell's demon and quantum-dot cellular automata. *J. Appl. Phys.* 2003, *94*, 1050–1060.

[23] Lu, Y.; Liu, M.; Lent, C. Molecular quantum-dot cellular automata: From molecular structure to circuit dynamics. *J. Appl. Phys.* 2007, *102*, 034311–1–6.

[24] Tokunaga, K. Signal transmission through molecular quantum-dot cellular automata: A theoretical study on Creutz-Taube complexes for molecular computing. *Phys. Chem. Chem. Phys.* 2009, *11*, 1474–1483.

[25] Remacle, F.; Levine, R.D. The time scale for electronic reorganization upon sudden ionization of the water and water-methanol hydrogen bonded dimers and of the weakly bound NO dimer. *J. Chem. Phys.* 2006, *125*, 133321–1–7.

[26] Remacle, F.; Levine, R.D. Time-resolved electrochemical spectroscopy of charge migration in molecular wires: computational evidence for rich electron dynamics. *J. Phys. Chem. C* 2007, *111*, 2301–2309.

[27] Tokunaga, K. Metal dependence of signal transmission through molecular quantum-dot cellular automata (QCA): A theoretical study on Fe, Ru, and Os mixed-valence complexes. *Materials* 2010, *3*, 4277–4290.

[28] Mulliken, R.S. Electronic population analysis on LCAO-MO molecular wave function, I. *J. Chem. Phys.* 1955, *23*, 1833–1840.

[29] Creutz, C.; Taube, H. Binuclear complexes of ruthenium ammines. *J. Am. Chem. Soc.* 1973, *95*, 1086–1094.

[30] Tom, G.M.; Creutz, C.; Taube, H. Mixed valence complexes of ruthenium ammines with 4,4′-bipyridine as bridging ligand. *J. Am. Chem. Soc.* 1974, *96*, 7827–7829.

[31] At the moment of the switch, $h^{\mathrm{f}}(0)$ is not exactly equal to h^{f} of Equation 2 because one-electron Hamiltonian itself depends on $|\psi_n\rangle$. After the switch, $h^{\mathrm{f}}(t)$ gradually approaches h^{f}.

[32] Szabo, A.; Ostlund, N.S. (1982) Modern Quantum Chemistry: Introduction to Advanced Electronic Structure Theory, Macmillan (New York).

[33] The $e^{i\,\Delta\varepsilon_{jj'}\,t}$ term gives not only cosine term but also sine term. The sine term is neglected in this work because imaginary charge represented by the term has no physical meaning.

[34] Frisch, M.J.; Trucks, G.W.; Schlegel, H.B.; Scuseria, G.E.; Robb, M.A.; Cheeseman, J.R.; Montgomery, Jr., J.A.; Vreven, T.; Kudin, K.N.; Burant, J.C.; Millam, J.M.; Iyengar, S.S.; Tomasi, J.; Barone, V.; Mennucci, B.; Cossi, M.; Scalmani, G.; Rega, N.; Petersson, G.A.; Nakatsuji, H.; Hada, M.; Ehara, M.; Toyota, K.; Fukuda, R.; Hasegawa, J.; Ishida, M.; Nakajima, T.; Honda, Y.; Kitao, O.; Nakai, H.; Klene, M.; Li, X.; Knox, J.E.; Hratchian, H.P.; Cross, J.B.; Adamo, C.; Jaramillo, J.; Gomperts, R.; Stratmann, R.E.; Yazyev, O.; Austin, A.J.; Cammi, R.; Pomelli, C.; Ochterski, J.W.; Ayala, P.Y.; Morokuma, K.; Voth, G.A.; Salvador, P.; Dannenberg, J.J.; Zakrzewski, V.G.; Dapprich, S.; Daniels, A.D.; Strain, M.C.; Farkas, O.; Malick, D.K.; Rabuck, A.D.; Raghavachari, K.; Foresman, J.B.; Ortiz, J.V.; Cui, Q.; Baboul, A.G.; Clifford, S.; Cioslowski, J.; Stefanov, B.B.; Liu, G.; Liashenko, A.; Piskorz, P.; Komaromi, I.; Martin, R.L.; Fox, D.J.; Keith, T.; Al-Laham, M.A.; Peng, C.Y.; Nanayakkara, A.; Challacombe, M.; Gill, P.M.W.; Johnson, B.; Chen, W.; Wong, M.W.; Gonzalez, C.; Pople, J.A. *Gaussian 03, Revision C.02*. Wallingford CT, 2004.

[35] Hardesty, J.; Goh, S.K.; Marynick, D.S. A comparative DFT-MP2 study of the Creutz-Taube ion and related systems. *J. Mol. Struct. (Theochem)* 2002, *588*, 223–226.

[36] Zhange, L.-T.; Ko, J.; Ondrechen, M.J. Electronic structure of the Creutz-Taube ion. *J. Am. Chem. Soc.* 1987, *109*, 1666–1671.

[37] Sizova, O.V.; Panin, A.I.; Ivanova, N.V.; Baranovskii, V.I. Electronic structure, spectrum, and intramolecular electron transfer model of $[(NH_3)_5Ru\text{-}(4,4'\text{-bipy})\text{-}Ru(NH_3)_5]^{5+}$. *J. Struct. Chem.* 1997, *38*, 366–374.

[38] Bencini, A.; Ciofini, I.; Daul, C.A.; Ferretti, A. Ground and excited state properties and vibronic coupling analysis of the Creutz-Taube ion, $[(NH_3)_5Ru\text{-pyrazine-}Ru(NH_{3)})_5]^{5+}$, using DFT. *J. Am. Chem. Soc.* 1999, *121*, 11418–11424.

[39] Broo, A; Larsson, S. Ab initio and semi-empirical studies of electron transfer and spectra of binuclear complexes with organic bridges. *Chem. Phys.* 1992, *161*, 363–378.
[40] Robin, M.B.; Day, P. Mixed valence chemistry - A survey and classification. *Adv. Inorg. Chem. Radiochem.* 1967, *10*, 247–422.
[41] Creutz, C. Mixed valence complexes of d5-d6 metal centers. *Prog. Inorg. Chem.* 1983, *30*, 1–73.
[42] Beattie, J.K.; Hush, N.S.; Taylor, P.R.; Raston, C.L.; White, A.H. Crystal structure of μ-pyrazine-bis(penta-ammineruthenium) penta-(bromide chloride)-water (1/4). *J. Chem. Soc., Dalton Trans.* 1977, 1121–1124.
[43] Fürholz, U.; Fürgi, H-.B.; Wagner, F.E.; Stebler, A.; Ammeter, J.H.; Krausz, E.; Clark, R.J.H.; Stead, M.J.; Ludi, A. The Creutz-Taube complex revisited. *J. Am. Chem. Soc.* 1984, *106*, 121–123.

IntechOpen



Cellular Automata - Innovative Modelling for Science and Engineering

Edited by Dr. Alejandro Salcido

ISBN 978-953-307-172-5
Hard cover, 426 pages
Publisher InTech
Published online 11, April, 2011
Published in print edition April, 2011

Modelling and simulation are disciplines of major importance for science and engineering. There is no science without models, and simulation has nowadays become a very useful tool, sometimes unavoidable, for development of both science and engineering. The main attractive feature of cellular automata is that, in spite of their conceptual simplicity which allows an easiness of implementation for computer simulation, as a detailed and complete mathematical analysis in principle, they are able to exhibit a wide variety of amazingly complex behaviour. This feature of cellular automata has attracted the researchers' attention from a wide variety of divergent fields of the exact disciplines of science and engineering, but also of the social sciences, and sometimes beyond. The collective complex behaviour of numerous systems, which emerge from the interaction of a multitude of simple individuals, is being conveniently modelled and simulated with cellular automata for very different purposes. In this book, a number of innovative applications of cellular automata models in the fields of Quantum Computing, Materials Science, Cryptography and Coding, and Robotics and Image Processing are presented.

How to reference

In order to correctly reference this scholarly work, feel free to copy and paste the following:

Ken Tokunaga (2011). Quantum-Chemical Design of Molecular Quantum-Dot Cellular Automata (QCA): A New Approach from Frontier Molecular Orbitals, Cellular Automata - Innovative Modelling for Science and Engineering, Dr. Alejandro Salcido (Ed.), ISBN: 978-953-307-172-5, InTech, Available from: http://www.intechopen.com/books/cellular-automata-innovative-modelling-for-science-and-engineering/quantum-chemical-design-of-molecular-quantum-dot-cellular-automata-qca-a-new-approach-from-frontier-

INTECH
open science | open minds

InTech Europe
University Campus STeP Ri
Slavka Krautzeka 83/A
51000 Rijeka, Croatia
Phone: +385 (51) 770 447
Fax: +385 (51) 686 166
www.intechopen.com

InTech China
Unit 405, Office Block, Hotel Equatorial Shanghai
No.65, Yan An Road (West), Shanghai, 200040, China
中国上海市延安西路65号上海国际贵都大饭店办公楼405单元
Phone: +86-21-62489820
Fax: +86-21-62489821

© 2011 The Author(s). Licensee IntechOpen. This chapter is distributed under the terms of the Creative Commons Attribution-NonCommercial-ShareAlike-3.0 License, which permits use, distribution and reproduction for non-commercial purposes, provided the original is properly cited and derivative works building on this content are distributed under the same license.

IntechOpen

IntechOpen